CrossMark

ORIGINAL PAPER

Removal of Tin from Extreme Ultraviolet Collector Optics by *In-Situ* Hydrogen Plasma Etching

Daniel T. Elg[1,4,5] · **Gianluca A. Panici**[1] · **Sumeng Liu**[2] ·
Gregory Girolami[2] · **Shailendra N. Srivastava**[3] · **David N. Ruzic**[1]

Abstract Extreme ultraviolet (EUV) lithography produces 13.5 nm light by irradiating a droplet of molten Sn with a laser, creating a dense, hot laser-produced plasma and ionizing the Sn to the $+8$ through $+12$ states. An unwanted by-product is deposition of Sn debris on the collector optic, which focuses the EUV light emitting from the plasma. Consequently, collector reflectivity is degraded. Reflectivity restoration can be accomplished by means of Sn etching by hydrogen radicals, which can be produced by an H_2 plasma and etch the Sn as SnH_4. It has previously been shown that plasma cleaning can successfully create radicals and restore EUV reflectivity but that the Sn removal rate is not necessarily limited by the radical density. Additionally, while Sn etching by hydrogen radicals has been shown by multiple investigators, quantification of the mechanisms behind Sn removal has never been undertaken. This paper explores the processes behind Sn removal. Experiments and modeling show that, within the parameter space explored, the limiting factor in Sn etching is not radical flux or SnH_4 decomposition, but ion energy flux. Thus the removal is akin to reactive ion etching.

✉ Daniel T. Elg
    daniel.elg@berkeley.edu

✉ David N. Ruzic
    druzic@illinois.edu

1   Department of Nuclear, Plasma, and Radiological Engineering, Center for Plasma-Material Interactions, University of Illinois at Urbana-Champaign, 216 Talbot Laboratory MC-234, 104 S. Wright St, Urbana, IL 61801, USA

2   Department of Chemistry, University of Illinois at Urbana-Champaign, 505 S. Matthews Ave., 104 S. Wright St, Urbana, IL 61801, USA

3   Applied Research Institute, University of Illinois at Urbana-Champaign, 2100 S. Oak St. Suite 206, Champaign, IL 61820, USA

4   Present Address: Department of Chemical and Biomolecular Engineering, University of California, Berkeley, 201 Gilman Hall, Berkeley, CA 94720, USA

5   Applied Materials, Inc., 3050 Bowers Ave, PO Box 58039, Santa Clara, CA 95054, USA

Introduction

In just the past 30 years, the minimum feature size on an integrated circuit has shrunk from
1 μm to 11 nm [1, 2]. Such rapid progress is what has enabled the semiconductor industry
to continue unabated exponential improvement for decades. Adherence to Moore's Law
has been made possible by advancements in lithography. Currently, the industrial work-
horse is optical lithography, which uses a 193 nm laser to pattern features on the Si wafer.
However, since the 11 nm minimum feature size is more than an order of magnitude
smaller than the 193 nm lithographic wavelength, time-consuming and expensive tech-
niques are needed in order to pattern such small features with such a comparatively large
wavelength.

Due to the small size of the shrinking half-pitch compared to the 193 nm wavelength, it
is desirable to develop a new lithographic technology based around a smaller wavelength
of light [3]. The most viable candidate for next-generation lithography uses 13.5 nm light,
which lies in the extreme ultraviolet (EUV) range and is produced by plasmas. Unfortu-
nately, EUV lithography must overcome a host of problems before reaching cost-effec-
tiveness. One key problem is collector optic contamination.

Collector contamination is caused by the interaction between the EUV light source and
the first piece in the optical chain: the collector optic. Due to the 92 eV energy of a
13.5 nm photon, EUV light must be made by a plasma, rather than by a laser. Specifically,
the industrially-favored EUV source topology is to irradiate a droplet of molten Sn with a
laser, creating a dense, hot laser-produced plasma (LPP) [4, 5] and ionizing the Sn to (on
average) the + 10 state [6, 7]. The optics for such sources are normal incidence multilayer
mirrors (MLMs). To overcome the high EUV absorption of all known solid materials,
MLMs employ synthetic Bragg reflection to reflect EUV light. This requires stacks of
∼ 7 nm-thick Mo/Si bilayers, which cause Bragg reflection of 13.5 nm light [6]. The first
of the mirrors is the collector optic, which collects the EUV light from the source and sends
it to the rest of the optical chain. Due to the absence of any known EUV-transparent
material of substantial thickness, the collector optic is exposed directly to the Sn plasma.

This Sn-based plasma emits Sn ion and neutral debris, which can damage the collector
optic in three ways: sputtering, implantation, and deposition. The first two damage pro-
cesses are irreversible and are caused by the high energies (1–10 keV) of the ion debris [8].
Debris mitigation methods have largely managed to reduce this problem by using colli-
sions with H$_2$ buffer gas to slow down the energetic ions. However, deposition can occur at
all ion and neutral energies, and no debris mitigation technique can deterministically
deflect all neutrals from the collector. Thus, deposition still takes place, lowering the
collector reflectivity and increasing the time needed to deliver enough EUV power to
pattern a wafer.

Deposition is a reversible process. However, a suitable cleaning technique must be
employed. Externally cleaning the collector requires both cost and significant source
downtime; therefore, it is desirable to clean the collector in situ, or inside the EUV source
chamber. Most in situ cleaning techniques employed in industry and studied in academia
have utilized etching by atomic H radicals [9–12], which chemically react with Sn to form
volatile SnH$_4$. However, these studies have been performed by utilizing a remote radical
source and then blowing the radicals at a Sn-coated sample. While this is a possible

technique, its application to a real EUV system could necessitate the insertion of a delivery system in front of the collector (causing downtime) and could be subject to radical diffusion and recombination on the walls of the delivery system in the chamber, significantly reducing the cleaning rate.

In a previous paper, a novel cleaning solution was proposed by using the collector itself to drive a capacitively-coupled hydrogen plasma, creating radicals directly on the collector surface. This technique was shown to completely clean a 300 mm-diameter dummy collector at 65 mTorr of H_2 and 300 W of power [13]. Additionally, it was shown to restore EUV reflectivity to Sn-coated MLMs without causing damage to the MLM surfaces. In another paper [14], H radical densities were shown to modestly increase with pressure (from 4.3×10^{12} cm^{-3} at 65 mTorr to 5.2×10^{12} cm^{-3} at 325 mTorr, with error bars between 10 and 20%). However, the etch rate decreased by about an order of magnitude over the same pressure range. This indicated that, within the parameter space explored, H radical density was not the limiting factor in Sn removal.

This paper provides an explanation of the fundamental process limiting Sn removal by H_2 plasma. While other papers have confirmed the ability to etch Sn with H radicals, a rigorous quantitative study of the removal rate limitation has not been previously undertaken. It is commonly postulated that the limiting factor in Sn removal is SnH_4 decomposition (and ensuing Sn re-deposition). Through theoretical and experimental means, this paper shows that hypothesis to be false for the etching system described in [13] within the current parameter space. Instead, it will be shown that removal rates in the plasma etching system are driven by the ion energy flux. This phenomenon is known as Reactive Ion Etching and implies that the main limitation is the necessity to break Sn–Sn surface bonds, allowing for H radicals to attach and form SnH_4. The presence of energetic ion bombardment also explains the ability of the plasma etching system to achieve "efficiency" values (measured in etched Sn atoms per incident H radical) an order of magnitude higher than those reported for hot-filament radical generators and plasma systems with low (~ 20 V) ion energies. The etching enhancement caused by energetic ions also has potential ramifications for industrial design of in situ Sn cleaning systems.

Experimental Setup

Plasma Etching Chamber

For plasma etching experiments, the Xtreme Commercial EUV Exposure Diagnostic (XCEED) chamber was utilized. Though originally a z-pinch EUV source, XCEED was repurposed to hold a 300 mm-diameter stainless-steel dummy collector, which was used to drive a capacitively-coupled H_2 plasma. The plasma was created by supplying 300 W of 13.56 MHz power to the collector, which was electrically isolated from ground. Figures 1 and 2 show the XCEED chamber with collector installed. This setup is described in further detail in [13].

To measure etch rates, a quartz crystal microbalance (QCM) coated with a thin film of Sn was used. The QCM was positioned directly on the collector. A typical etch was measured by reading the QCM thickness beforehand, disconnecting the transducers from the QCM feedthrough flange, running the etch, and reconnecting the transducers and reading a new thickness after turning off the plasma. Etch rate was then calculated by
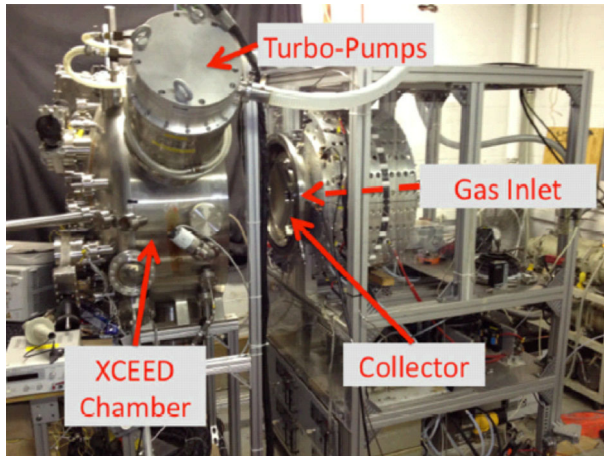
Fig. 1 XCEED is shown with the collector installed. For etching experiments, the chamber (on the cart at left) was attached to the former EUV source (at right). The collector was driven with 300 W 13.56 MHz RF power through an electrical feedthrough, which allowed for electrical connection to the electrically isolated dummy collector
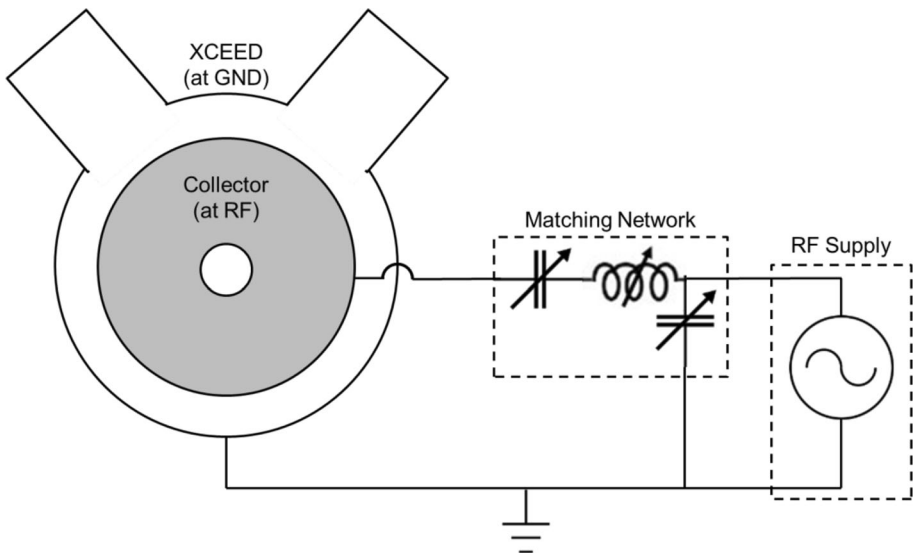

Fig. 2 The etching plasma circuit diagram is shown. The collector is isolated from ground inside XCEED and is attached to a 300 W 13.56 MHz RF supply. Reflected power is minimized by a matching network

dividing the thickness difference by time. Unless otherwise noted, the etch time used in this paper was 5 min.

Three other in situ diagnostics were also present in XCEED: a Langmuir Probe (to measure electron density, n_e, and electron temperature, T_e), a catalytic radical probe (to measure H radical density) [15–17], and a high-voltage probe attached to the RF feed-through of the collector (to measure the collector potential). Operation of the Langmuir probe is described in Ref. [18], while operation of the radical probe is described in Refs.

[14–17]. The Langmuir and radical probes were mounted on a transfer arm that allowed for precise positioning in the z-axis, as described in Ref. [14]. The collector had a 15 cm outer radius and a 3 cm inner radius. Thus, most measurements were taken at a radius of approximately 10 cm, near the middle of the collector. However, for certain experiments, the probes were moved to the inner and outer edges of the collector.

Deposition of Stannane (DOS) Chamber

An experimental setup was built to allow quantification of Sn redeposition probability on a Sn surface. This setup consisted of a glass vacuum chamber with a Sn-coated QCM. The chamber was made of glass because SnH_4 does not easily decompose on glass [11, 19–21]. DOS was pumped by a roughing pump to a base pressure of approximately 10 mTorr. Successive Ar purges were then used to lower the partial pressure of air in the chamber. All metal components, except the exposed Sn-coated QCM surface, were covered with fiberglass tape in order to minimize decomposition on surfaces other than the QCM.

The chamber was equipped with a gas-independent MKS Baratron 722 Capacitance Manometer. The QCM holder was also equipped with water lines, which were used to heat the QCM. Fluid (water for low temperatures, ethylene glycol for high temperatures) heated by a hot plate was pumped through the water lines by a small 12 V water pump. Once base pressure was reached and Ar purges were completed, the system was isolated from the vacuum pump and exposed to a source of SnH_4. The operating SnH_4 pressure was approximately 10 Torr, and deposition was measured with the QCM. A diagram of DOS is shown in Fig. 3.

Since SnH_4 is unstable and rarely-prepared, it was synthesized rather than purchased for these experiments. The synthesis was carried out in a manner similar to that described by Norman [22]. By slowly adding $SnCl_4$ to $LiAlH_4$ dissolved in diethyl ether at -65 °C, the following reaction was carried out:
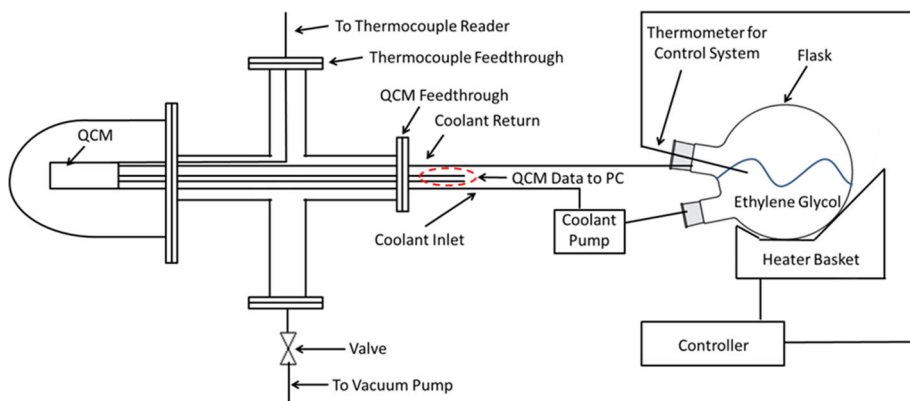

Fig. 3 A labeled diagram of the final DOS setup is shown. For high-temperature operation, water was replaced with ethylene glycol, which is placed in a 2-necked flask and heated. The pump used to circulate the ethylene glycol is positioned below the flask in order to keep it primed. The fluid returns to the flask through the second (upper) neck. The heater basket is controlled with an on–off ("bang–bang") controller. A thermocouple measures the QCM temperature, and a Baratron measures the pressure. The Baratron and the glass-metal joint leading to the SnH_4 source are not shown in this 2D diagram, since they are located on the front and back of the cross

$$SnCl_4 + LiAlH_4 \rightarrow LiCl + AlCl_3 + SnH_4. \tag{1}$$
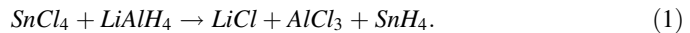
While SnH_4 is the only gaseous product in Eq. (1), it was contaminated by ether vapor. Ether vapor was removed with a cold-finger reflux condenser and a $-95\ °C$ U-trap. SnH_4 was then collected by condensation to a solid in liquid N_2-cooled traps; since the gaseous phase can decompose at any temperature, it was then stored in solid form in a liquid N_2 bath until evaporation for use in DOS.

Sn Thin Film Deposition

DC magnetron sputtering with Ar^+ ions was used to deposit Sn thin films on the QCMs used in XCEED and DOS. Deposition was carried out in a small $6''$ cross grafted onto XCEED. Due to the small size of the chamber, the $2''$-diameter magnetron was only approximately 2 cm from the QCM surface. Deposition current and pressure were generally 100 mA and 30 mTorr, though these parameters were sometimes altered to prevent oxidation of the Sn target and ensuing film. Due to the strong affinity of Sn for oxygen, the presence of adsorbed water on the walls of a small device with a high surface area-to-volume ratio, and a base pressure of only 10^{-6} Torr, oxidation of the Sn sputtering target could create impurities in the deposited film. To guard against this, several steps were implemented [23], primarily using short pulsed depositions (5 s of deposition, followed by 90 s of off-time) to maintain a cool target temperature and avoid the fast Sn oxidation rates seen at high temperatures [24].

X-ray photoelectron spectroscopy (XPS) of samples deposited without these precautions showed highly-oxidized films, and the target surface was visibly oxidized. In contrast, XPS of samples deposited in this method showed very small oxygen contents comparable to those seen in samples of pure Sn with room-temperature native oxide. Samples from contaminated depositions with bulk oxidation were observed to consistently etch more slowly than those with XPS signals comparable to pristine Sn samples. Additionally, while etching of Sn oxides has been observed in the literature, etch rates have usually either shown to be slower or negligible to compared to those for pure Sn, or simply not compared to those for pure Sn [25–28]. Nevertheless, it should be noted for the sake of completeness that there is still some disagreement in the literature as to whether oxidation of an Sn film inhibits etching.

For some experiments, the entire dummy collector was coated with Sn. The Sn deposition for the collector was carried out in a large system called GALAXY [29] which contained a $14''$-diameter sputtering target and used a current of 2.3 A, resulting in a higher current density. To attempt to minimize oxidation, the same pulsing technique was used.

SnH_4 Transport and Redeposition Theory

In a previous paper, it was discovered that, within the given parameter space, radical density was not the limiting factor in H_2 plasma removal of Sn. When the pressure increased from 65 to 325 mTorr, etch rate decreased from 1.1 nm/min to less than the error range of the profilometer (approximately 0.25 nm/min), even though the radical density saw only a slight increase [14]. Therefore something else must be responsible for the decrease in etch rate. One potential mechanism is redeposition. If the SnH_4 decomposes readily in the gas phase due to collisions with the background gas, or in collisions with the

collector itself, the net etching rate would be reduced. To determine the re-deposition rate it was necessary to develop a model to solve for the density profile of SnH_4.

In order to know the density profile of SnH_4, it was necessary to solve a fluid equation for SnH_4 density that took into account the processes of SnH_4 transport, creation, and destruction. The use of a fluid equation was justified by calculation of a Knudsen number of 0.005 at 65 mTorr; this number decreased at higher pressures. For Knudsen numbers less than 0.01, the gas is in the viscous flow regime, allowing for a continuous approximation and the use of fluid equations as opposed to Monte Carlo simulations of individual particle trajectories [30].

Physically, the relevant processes for the fluid equation are as follows and correspond to transport, creation, and destruction of SnH_4. In order to investigate if flow had any effect on the SnH_4 profile (and subsequent redeposition), it was necessary to consider SnH_4 transport in the volume not only by diffusion but also flow-driven advection. Creation of SnH_4 does not occur in the chamber volume; it occurs only at the collector surface and is caused by etching. The work of Tamaru [19] showed that SnH_4 decomposition does not occur upon collision with gas molecules; it occurs only on wall surfaces, not in the volume. The only other source of SnH_4 "destruction" is for the gas to leave the volume through the pumping system. Thus, destruction, like creation, only occurs at boundaries.

Accordingly, to obtain the SnH_4 density profile, the steady-state diffusion–advection equation with no source is solved [Eq. (2)], where n is the density of SnH_4, D is the diffusion coefficient, and $\mathbf{v}$ is the flow-driven gas velocity:

$$\frac{\partial n}{\partial t} = 0 = -\nabla \cdot (D\nabla n) + \mathbf{v} \cdot \nabla n. \tag{2}$$

Since creation and destruction only occur at surfaces, they enter the math as boundary conditions for Eq. (2) and are described by fluxes into and out of surfaces. The boundary condition for SnH_4 creation is applied to the collector surface and is given by Eq. (3), where $\mathbf{n}$ is the surface normal vector and Γ_{etched} is the flux of SnH_4 lifted from the collector by etching. This is the flux of etched SnH_4 that would be measured in the absence of redepostion.

$$-D\frac{\partial n}{\partial \boldsymbol{n}} = \Gamma_{etched}. \tag{3}$$

The redeposition boundary condition can be written in the same form as Eq. (3); however, the redepositing flux will be given as a fraction of the SnH_4 flux incident on the surface. Thus, it will be proportional to the SnH_4 density, as shown in Eq. (4):

$$-D\frac{\partial n}{\partial \boldsymbol{n}} = \Gamma_{redepositing} = \gamma\frac{1}{4}nv_{th} \tag{4}$$

where v_{th} is the thermal velocity and γ is the redeposition coefficient. This coefficient is the probability of a SnH_4 molecule decomposing when it strikes the collector. A real contaminated EUV collector will not simply contain Sn only at one point. Additionally, the collector used in this dissertation was fully coated with Sn. Therefore, it will be assumed in the model that the collector surface is coated with Sn; accordingly, the relevant γ is that associated with SnH_4 decomposition on a Sn surface.

Thus, the boundary condition for the collector surface is a superposition of Eqs. (3) and (4). The diffusion coefficient D for Eqs. (2)–(4) is found by means of Eq. (5), where λ is the neutral–neutral mean free path:

$$D = \frac{\pi}{8} \lambda v_{th}. \tag{5}$$

A 3D model was set up in COMSOL to solve Eq. (2) using the "Transport of Diluted Species" module. However, the model required 3 main external inputs. One was the velocity flow profile **v**, which was obtained by solving the Naiver-Stokes equations with the Laminar Flow module. The assumption of laminar flow, rather than turbulent flow, was justified by the need of a Reynolds number greater than 2000 for turbulent flow. Such a high Reynolds number was achievable only with unphysically high flow velocities of 13,000 m/s; thus, it was safe to assume that the flow remained in the laminar regime. Since the most predominant species in the chamber (by orders of magnitude) was neutral H_2 [14], it was assumed that SnH_4 molecules simply assumed the flow profile of H_2 without disturbing it. Thus, momentum balance could be decoupled from mass balance, and the Navier–Stokes equations were solved only once for H_2. This is similar to approaches seen in other works on neutral transport in plasmas [31, 32].

The other inputs necessary for the theoretical model were the redeposition coefficient and the "raw" etching rate (without redeposition). These values were determined through investigations in the following sections. It will be shown that the redeposition coefficient is very small and that etch rates are governed by the ion energy flux (reactive ion etching).

Redeposition Coefficient

In order to know if redeposition would play a large role in determining the net SnH_4 removal rate, it was necessary to know the redeposition coefficient, which is the probability of an SnH_4 molecule dissociating and depositing Sn upon impact with a wall. The most in-depth study of this phenomenon in the literature was performed by Tamaru, who observed the decomposition of SnH_4 in a glass chamber as a function of time and SnH_4 partial pressure.

In that paper, it was observed that SnH_4 did not easily decompose on a glass surface and only began to measurably do so once the surface was coated in Sn. In addition, by plotting the partial pressure of SnH_4 as a function of time on a logarithmic scale, a reaction rate coefficient was calculated from the slope of the resulting line. This reaction rate was independent of initial pressure. Thus, it was observed that SnH_4 does not dissociate upon impact with neutral gas atoms in the volume; additionally, it was shown that SnH_4 decomposes vary slowly on a glass surface compared to a Sn surface; this finding is similar to that of Ugur, who showed that SnH_4 decomposed slower on oxides than on metals [11].

Tamaru also observed that the measured reaction rate was highly temperature-dependent an obeyed an Arrhenius behavior. However, the reported decomposition probabilities were in the form of reaction rates measured in units of min^{-1}. This is due to the values being reported as reaction rates satisfying the following first-order chemical decay equation [Eq. (6)], where k_d is the reaction rate and n is the density of SnH_4:

$$\frac{dn}{dt} = -k_d n. \tag{6}$$

To convert the reaction rates into unit-less redeposition probabilities, it was necessary to re-write Eq. (6). While Eq. (6) is mathematically true, it should be noted that such a form is typically used to describe volumetric decay in chemical reactions. Since the decomposition reaction is actually a boundary surface reaction, writing it in the form of Eq. (6)

incorporates information about the walls of the particular reactor; to avoid this, it may be written as a surface boundary reaction, as in Eq. (7):

$$\frac{dn}{dt} = \frac{A}{V}\Gamma \tag{7}$$

where A and V are the surface area and volume of the chamber and Γ is the flux of SnH_4 leaving the volume by means of decomposition on the walls. This term is given in Eq. (8), where γ is the redeposition coefficient:

$$\Gamma_{boundary} = \gamma \Gamma_{SnH_4} = \gamma \frac{1}{4} n v_{th} \tag{8}$$

Plugging Eq. (8) into Eq. (7), equating Eq. (7) with Eq. (6), and re-arranging terms gives Eq. (9) for the redeposition probability:

$$\gamma = \frac{4}{v_{th}} k_d \frac{A}{V}. \tag{9}$$

The steady-state collector temperature during plasma etching in XCEED was measured by a thermocouple to be 165 °C at 65 mTorr and 120 °C at 325 mTorr, respectively. Extrapolating the Arrhenius plot from Tamaru's paper and converting the resulting reaction rates into redeposition probabilities yielded $\gamma = 3.7 \times 10^{-6}$ at 165 °C and $\gamma = 6.8 \times 10^{-7}$ at 120 °C. Thus, the probability of redeposition is very low at the conditions used in this paper, suggesting that SnH_4 redeposition may be insignificant and may not be the limiting factor during plasma etching in XCEED.

To verify such low orders of magnitude for γ, experiments were carried out in DOS. After the evacuation procedure described in "Experimental Setup" section, SnH_4 was inserted into the chamber, usually resulting in a pressure of 5–6 Torr. As described in "Experimental Setup" section, a Sn-coated QCM was used to measure deposition at controllable temperatures, which were achieved by heating ethylene glycol and pumping it through the water cooling lines of the QCM setup. At 20, 35, and 50 °C, no measurable deposition occurred. The maximum operating temperature was limited to 110 °C by failure of the ethylene glycol pump. Even at this temperature, no measureable redeposition generally occurred. In one particular experiment, a deposition that was linear in time appeared to occur for approximately 4.5 min, though it was preceded and succeeded by fluctuations and noise. Even in this case, calculating the slope of the deposition curve yielded a calculated deposition rate of only 0.0044 A/s, which is below the noise floor of the instrument. Using Eqs. (7) and (8) to calculate the corresponding redeposition probability yields a probability of only 10^{-9}. Thus, though these experiments were unable to provide independent measurements of redeposition probabilities, they did confirm that such probabilities are very small. For the rest of this paper, the values found in the work of Tamaru will serve as an upper bound of the redeposition probability.

Reactive Ion Etching of Sn

As previously mentioned, etch rates on a Sn-coated collector were observed to significantly decrease when the pressure was increased, even though the density of etchant H radicals slightly increased. While it had often been suspected that increased Sn redeposition at low mean free paths was to blame for this, the results of "Redeposition Coefficient" section

indicated that redeposition was likely not as important as had once been thought. Thus, it was desirable to perform an in-depth study of etching processes. In addition, to complete the SnH_4 transport model from "SnH$_4$ Transport and Redeposition Theory" section and definitively calculate whether or not redeposition was a limiting factor in Sn removal, it was necessary to measure "raw" etch rates without any redeposition.

Thus, XCEED was set up as described in "Sn Thin Film Deposition" section. Though previous work involved a Sn-coated collector [13, 14] the work presented here was performed with a clean collector; to minimize the potential for redeposition, the only source of Sn was an 8 mm Sn-coated QCM used to measure etch rates. The QCM was coated with 460 nm of Sn, and the purity of the Sn film was verified with XPS. Though a surface profilometer had been used previously to quantify etch rates [13, 14], the QCM allowed for in situ calculation of etch rates with smaller error bars and shorter etch times (most etches in this paper were 5 min long, as opposed to 2 h in previous studies).

Constant, Time-Invariant Etch Rates and Sn Island Effect

The first test performed was to see if a constant etch rate could be produced. Before looking at etch rates from a variety of conditions, etch rate consistency will be shown through individual etches at one condition on one crystal. A long series of etches, mostly 5 min long, were performed at 65 mTorr and 300 W with the Langmuir probe and QCM at a radial position of approximately 10 cm. The QCM thickness was measured after every etch. Breaking the etching process up into these small intervals allowed for a determination of if the etch rate was changing in time or not. The results from this series of etches is shown in Fig. 4. On this scale, the error bars are smaller than the markers. The time shown on the x-axis is the cumulative amount of time spent etching.

Figure 4 displays a high degree of linearity in the etching, with a constant etch rate being maintained for the entire 2.5 h of etching. As another indication of linearity, the etch rates for each individual etch are presented in Fig. 5.

The etch rate data in Fig. 5 show no trend after 2.5 h. Averaging the data points in Fig. 5 yields an average etch rate of 1.75 nm/min. Mean while, fitting a line to the data in Fig. 4 yields a slope of 1.72 nm/min. This similarity between the mean etch rate and the slope of the fit line is another indicator of a constant etch rate, measurement reliability, and experimental reproducibility. Error bars of approximately ± 18% are derived from the

Fig. 4 Over 2500 Å (250 nm) were etched in XCEED at 65 mTorr and 300 W. The runtime for most etches was 5 min. This linear etch indicates a constant etch rate in XCEED. Error bars are smaller than the markers. The etch rate remained constant over an etch time of approximately 2.5 h
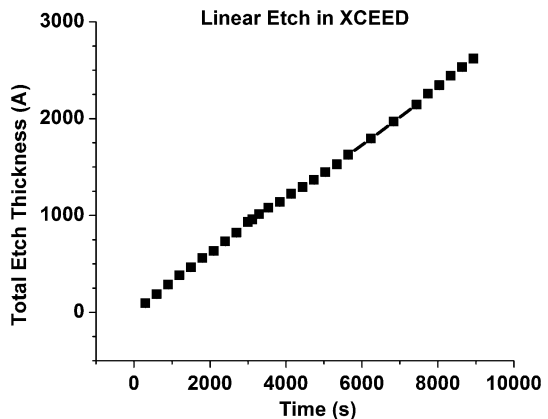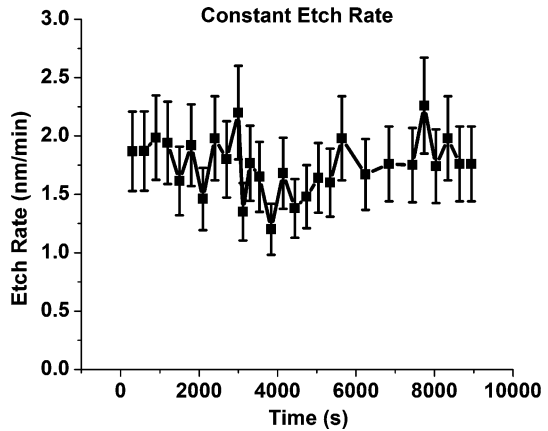
Fig. 5 The etch rates for the etches shown in Fig. 4. No trend is observed over 2.5 h. Error bars are approximately 18% and come from a standard deviation of etch rates

standard deviation of etch rates across many QCMs etched at 65 mTorr and 300 W, which had an average etch rate of 1.9 nm/min. It should also be noted that the data in Figs. 4 and 5 include some etches that were 3, 4, and 10 min long. These etches showed no dependence of etch rate on etch time.

Finally, a form of thickness dependence was observed. It was observed that after etching approximately 3000 Å of the 4600 Å film, the etch rate dropped to approximately 1.2 nm/min. Due to the purity of the Sn film and the lack of any change in etch rate for the first 3000 Å, the most likely reason for this drop is that pieces of the Au-coated crystal under the Sn have become exposed. For the thick films deposited in this work, these islands grow up and out, joining together; however, the film's shape and local thickness remain affected by the original islands. This was confirmed by atomic force microscopy (AFM) images of deposited films. Essentially, due to the deposition mechanism, some parts of the film are thicker than others. However, if etching preferentially proceeds in a vertical direction (which, as will be discussed later, is a reasonable assumption), then the thinner areas of the film will be etched to completion faster than the rest of the film, effectively separating the islands. While the islands will continue to etch, the spaces between them will not; effectively, the surface coverage of Sn is less than 100%, and the probability of plasma species interacting with Sn is decreased. This is the most likely cause of the decreased etch rate seen after reaching the last 160 nm of the deposited film. Finally, it should be noted that Au may also have a different catalytic effect than Sn on SnH_4 decomposition, potentially raising the redeposition rate.

The role of incomplete Sn coverage in lowering Sn etch rates is corroborated by XPS measurements, which displayed Sn peaks without Au peaks before etching (indicating a closed Sn surface) and Au peaks in addition to Sn peaks after 300 nm of etching (indicating that part of the underlying Au surface of the QCM was exposed). Additionally, this concept of voids between Sn islands is seen in post-etch secondary electron microscopy (SEM) images of a post-etch surface in [13], which had an original Sn thickness of 200 nm that was etched down to a thickness of 65 nm (measured by a profilometer). It should be noted that that etch, which was performed on a Sn-coated collector, yielded an average etch rate of 1.1 nm/min, which is within error of the 1.2 nm/min for the last 150 nm of the Sn-coated QCM exposed to the same conditions in XCEED. Thus, this similarity between removal rates on a coated and a non-coated collector reinforces that redeposition is small

or negligible. For other etches performed in this paper, the Sn film was kept sufficiently thick such that the thickness-dependent drop in etch rate was avoided.

Parameter Variation and Ion Energy Flux Dependence

Having set up an in situ etch rate measurement system and verified a constant etch rate, parameter variation was explored in order to understand the effect of various parameters on etch rate. While one parameter was varied, the other parameters were kept at their base values (65 mTorr, 300 W, 1000 sccm flow, and 10 cm radial position). Additionally, for each set of parameter variation experiments, a "check-in" at the base condition was performed to verify that etching was occurring in the same manner for every QCM used.

Variation of power showed a linear dependence of etch rate on power between 100 and 300 W. This is similar to the linear variation of radical density with power shown in Ref. [14]. Etch rate and radical density, normalized to their values at 300 W, are plotted in Fig. 6.

However, when pressure was varied instead of power, the etch rate was nonlinear with pressure and did not follow the radical density, as shown in Fig. 7. The order-of-magnitude drop in etch rate between 65 and 325 mTorr seen in previous full-collector experiments [13, 14] was reproduced in the absence of redeposition with only the Sn-coated QCM. Thus, something other than radical density and redeposition was the limiting factor in etch rate.

At this point, the task was to identify the limiting factor. The answer lay in looking not for a limiting factor but an enabling factor. The works of Ugur, Braginsky, and van Herpen [9–12] had both shown etching probabilities of only 1 SnH_4 molecule for approximately every 10^5 incident H radicals. However, the etch rate in XCEED at 65 mTorr and 300 W (1.9 nm/min) produced an SnH_4 molecule for approximately every 2300 incident H radicals. Clearly, something in XCEED enables a much more efficient etching process.

The common link between the MSWP experiments and the works of Ugur, Braginsky, and van Herpen was a lack of energetic ion bombardment. While the work of Braginsky had used plasma-created H radicals, the ion energies were very low, near 10 eV; this, combined with the small mass of hydrogen ions, allowed for very little energy delivery to the Sn by ion bombardment. It is hypothesized that a threshold energy effect was

Fig. 6 The etch rate and radical density are normalized to their values at the base condition (65 mTorr, 300 W) and plotted together. Both follow the same linear trend with power
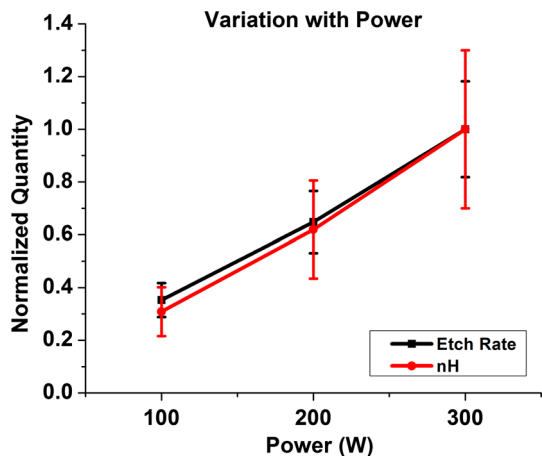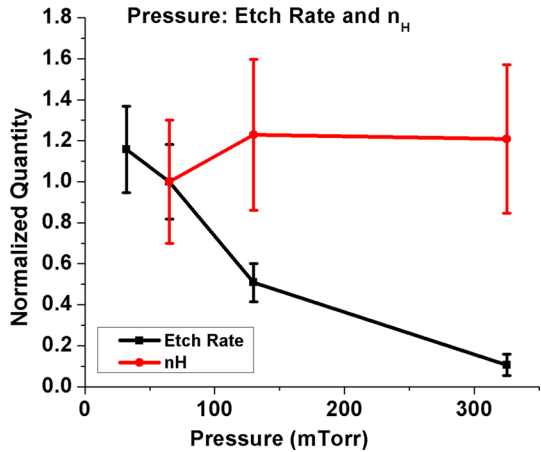
Fig. 7 When the pressure is
varied, the etch rate does not at
all follow the radical density.
Therefore, the factor limiting the
etch rate is neither redeposition
nor radical density

responsible for the lack of observed ion enhancement in Braginsky's work. Ugur and van Herpen, meanwhile, utilized plasma-less atomic hydrogen sources.

Ion-enhanced etching is a well-known phenomenon often exploited in semiconductor processing, but it has not previously been studied in H_2 etching of Sn. Physically, ion-enhanced etching (also known as "reactive ion etching", or RIE) raises etch rates because the incident ions break bonds between surface molecules. Without those bonds broken, the likelihood of etchant radicals chemically reacting with the surface is often quite low; if energetic ions are present, however, the plasma sheath directs them into the surface, causing them to break bonds upon impact. Radicals can then much more easily attach to these "dangling" bonds. Thus, the quantity governing RIE should be correlated to the number of bonds being broken. The most logical quantity is the ion energy flux, which is the product of the incident ion flux and the average ion energy. The energy dictates the chances of an incident ion breaking a bond (or multiple bonds), while the flux provides a measurement of how many energetic ions are striking the surface per second.

Since ions in the cold plasma are assumed to be at the gas temperature and electric fields are weak in the bulk plasma, ion impact energy is acquired due to transit through the plasma sheath. Thus, average ion energy was calculated by finding the difference between the plasma potential (measured with the Langmuir probe) and the average surface potential (measured with the high-voltage probe), which displayed a negative DC self-bias characteristically seen on the smaller electrode of RF capacitively-coupled plasmas [33]; in this case, the collector was the smaller electrode because the ground electrode consisted of the entire chamber. Ion flux was calculated from the ion saturation current measured with the Langmuir probe. Since current is itself a flux and all ion current to a Langmuir probe is conduction current rather than displacement current, the current density J can be written simply as a charged, directed flux as seen in Eq. (10), where q_e is the electronic charge, n is the ion density, and v is the ion velocity:

$$J = q_e n v. \tag{10}$$

After noting that J is simply the ion saturation current (I) divided by the probe area (A) the flux, nv, may then be solved for [Eq. (11)]:

$$\Gamma_{ions} = nv = \frac{I}{Aq_e}.$$ (11)

It should be noted that, at 325 mTorr, the sheath becomes collisional and the probe enters the collisional regime. However, since the ion flux is simply the current divided by the probe area and the electronic charge, a collisional sheath does not inhibit the ability to measure ion flux. The collisional sheath does make it difficult to back-calculate the bulk ion density from that flux, but the flux itself can still be measured by means of Eq. (11).

The ion energy flux (IEF) is then given as the product of the flux and the energy (E_i), as seen in Eq. (12):

$$IEF = E_i \frac{I}{Aq_e}.$$ (12)

Figure 8 indicates that the RIE theory captures the etch rate behavior in pressure quite well, showing the etch rate and IEF overlapping when normalized to the etch rate at 65 mTorr.

It is not surprising that the IEF decreases as pressure increases. An increase in pressure (within this pressure range) causes a decrease in electron (and, therefore, ion) density in the plasma. Meanwhile, at high pressures, the sheath becomes small. The size of a capacitive plasma RF sheath is inversely proportional to the displacement current through the sheath [33]. Thus, as the sheath becomes small, the conduction current is allowed to decrease resulting in fewer ions transiting the full sheath to the collector. Finally, it should be noted that ion current through the 325 mTorr sheath is also inhibited by collisions. While the Langmuir probe can measure this current, collisions in the sheath can also decrease the energies of transiting ions, causing final energies to be somewhat less that the potential drop and reducing the etch rate; this effect could explain why there is slightly more separation between the normalized etch rate and normalized apparent ion energy flux at 325 mTorr than at lower pressures.

If IEF is indeed the limiting factor in the Sn etch rate, it should govern etch rate when all parameters, not just pressure, are varied. To further confirm the crucial role of IEF, Fig. 9 shows the etch rate to track the IEF when power is varied. This also illustrates why the etch

Fig. 8 Over a pressure range of two decades, the etch rate is shown to track the ion energy flux. This indicates that ion energy flux is the limiting factor in this regime and that etching enhancements take place due to ion bombardment
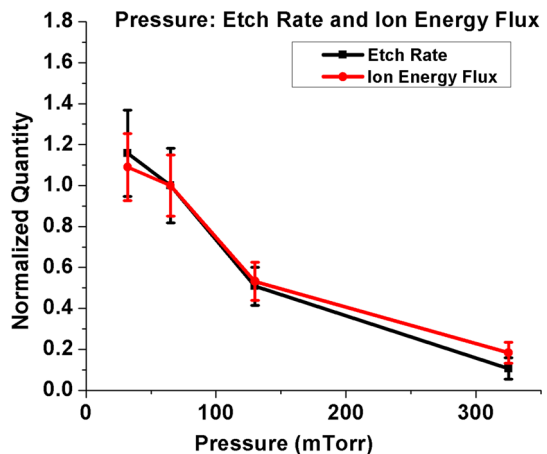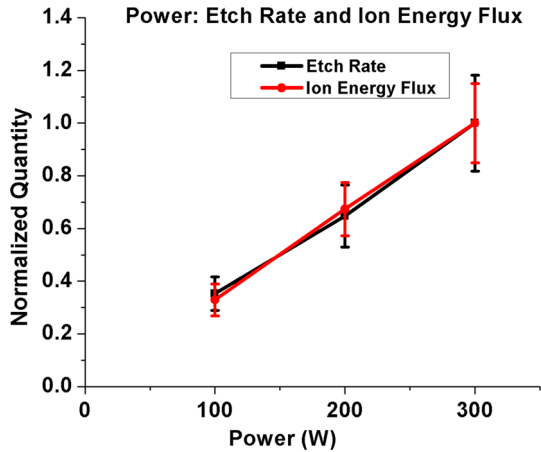
Fig. 9 The etch rate tracks the ion energy flux as a function of power. This explains why the etch rate varied in the same manner as radical density in Fig. 6, as radical density and IEF are both linear in power


rate appeared to follow the same trend as radical density in Fig. 6; both radical density and IEF are linear in power.

It is not surprising that the ion energy flux, which is a product of a current and a voltage, is proportional to power. In fact, if the electronic charge term is removed from Eq. (12), the ion energy flux can mathematically be written as a power density. However, it should be noted that this is not the total power density on the collector. For example, at 65 mTorr, dividing the ion current by the probe area, multiplying by the collector area, and multiplying by the ion energy yields approximately 1000 W on the collector. This is certainly larger than the measured total 300 W power on the collector. This difference is due to the fact that the total current on the collector is not solely ion current; there is also electron current and displacement current that can oppose the ion current. For example, as the voltage on the collector oscillates, the sheath changes in size and potential; for low instantaneous sheath potentials, few ions transit to the collector, while fast electrons easily reach the collector. Thus, the total current (and the total power) on the collector is less than that which would be predicted by ion current alone [34].

Two other parameters were varied to confirm the governing nature of IEF. The first parameter, flow, expectedly did not alter the ion density or ion energy. Accordingly, no variation in etch rate was seen when flow was varied between 500 and 1000 sccm. The other parameter was the position of the QCM on the collector, since gradual variations in n_e occur over the surface of the collector. The trends in etch rate and IEF once again overlap, as shown in Fig. 10; both quantities are normalized to their values at 10 cm. It should be noted that, while the QCM and Langmuir probe were moved to the positions shown in Fig. 10, the location of the high-voltage probe on the RF feedthrough outside the chamber (rather than on a particular point on the collector) caused an inability to measure any spatial variations in collector potential. Low-voltage tests conducted at atmosphere by opening the chamber and physically touching the probe to different spots on the collector indicated only minor variations in potential; however, these tests were conducted without any plasma present. Since the collector is a conductor, significant changes in its average potential drop are not expected.

Finally, it should be noted that, as discussed previously, the temperature of the collector varied from 165 °C at 65 mTorr to 120 °C at 325 mTorr, with convective cooling causing a decrease in temperature with a rise in pressure. There is disagreement in the literature

Fig. 10 The etch rate is shown
to vary with position. This is due
to lower electron densities away
from the center of the collector.
Etch rate and IEF continue to
follow each other
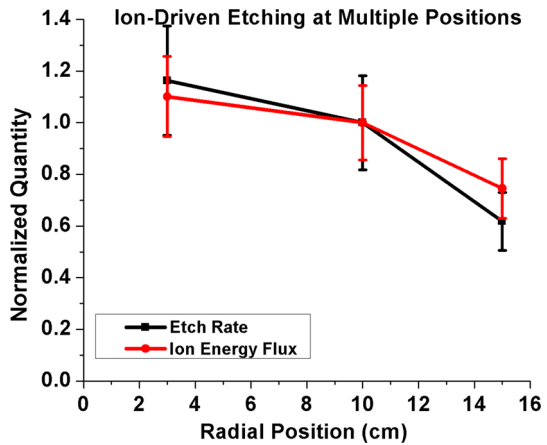
about the expected effect of temperature on the etch rate [25, 35], and it would be useful to examine temperature as a controlled variable in future work.

Insignificance of Redeposition

Redeposition Model Results

With raw etch rates now known, the last piece of information needed to run the diffusion–advection model described in "SnH$_4$ Transport and Redeposition Theory" section was complete. The model was solved for the SnH$_4$ density as described in "SnH$_4$ Transport and Redeposition Theory" section for both 65 and 325 mTorr to investigate pressure extremes while using raw etch rates at measured at 300 W for both pressures. At both pressures, the flow rate was set to the experimental value of 1000 sccm. Cross-sectional top-down SnH$_4$ density profile results are shown in Figs. 11 and 12, with the inlet at the back and the pumps shown as cylinders protruding from the chamber. The collector is positioned in front of the gas inlet, and the front surface of the collector serves as the source of SnH$_4$.

In Figs. 11 and 12, the peak SnH$_4$ density at 65 mTorr is 4.6×10^{17} m^{-3}, while the peak SnH$_4$ density at 325 mTorr is 2.4×10^{17} m^{-3}. In transitioning between the two pressures, the SnH$_4$ density decreased by approximately a factor of 2. This is not surprising, since the etch rate dropped by a factor of 10 (1.9–0.2 nm/min) but the pressure increased by a factor of 5, decreasing the mean free path proportionally and increasing SnH$_4$ confinement near the collector surface. Though the redeposition coefficient changed by a factor of approximately 5, this does not seem to have much of an effect, since the redeposition coefficient is so small.

Given the calculated densities of SnH$_4$, Eq. (13) was carried out to determine the expected deposition rates on the collector:

$$Deposition\,Rate = \frac{1}{4}\gamma \frac{n v_{th}}{n_{Sn}}. \tag{13}$$

At 65 mTorr, this yields an expected deposition rate of 1.8×10^{-4} nm/min; at 325 mTorr, the expected deposition rate is 1.7×10^{-5} nm/min. These values indicate that
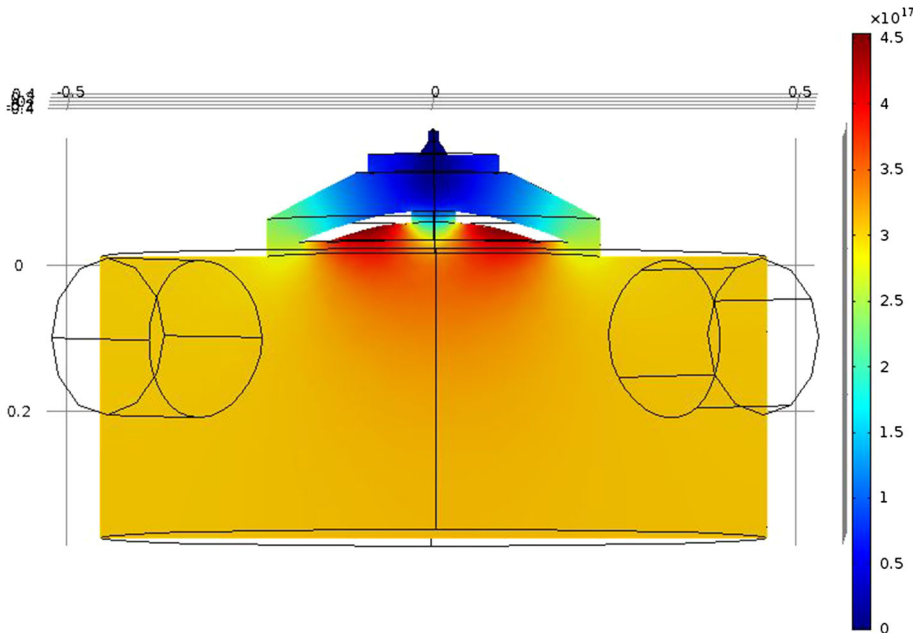
Fig. 11 The simulated SnH_4 density profile from the model in "SnH_4 Transport and Redeposition Theory" section is shown at 65 mTorr, 1000 sccm. At this pressure, the etch rate is 1.9 nm/min, and the temperature is 165 °C. The redeposition coefficient is 3.6×10^{-6}. The peak simulated SnH_4 density at the collector surface is 4.6×10^{17} m^{-3}

redeposition should be far below the measurable range on the QCM and should not noticeably affect net removal rates.

As a check of the insignificance of redeposition, exploration of flow variation was carried out with the model. Any effect of redeposition was expected to be altered by flow; high flow rates can blow away SnH_4 quickly, allowing less time for potential redeposition, while low flow rates allow SnH_4 more chances to collide with the collector before being pumped out. By lowering the flow at 65 mTorr to 560 sccm, the profile in Fig. 13 was achieved, where the maximum SnH_4 density is 7.7×10^{17} m^{-3}. The redeposition rate rose to 3.6×10^{-4} nm/min, but this value is still far below what can be detected by the QCM, and redeposition does not significantly lower the net removal rate in comparison to the raw etch rate.

Additionally, the flow at 325 mTorr was increased in the model to 3200 sccm, which is the highest flow rate that the XCEED pumps can handle while keeping the pressure at 325 mTorr. This was done to show that simply raising the flow rate cannot significantly raise the removal rate, since the limiting factor is IEF rather than redeposition. The resulting profile is shown in Fig. 14. Though flow obviously affects the SnH_4 density profile, this effect does not translate into an increase in net removal rate, since the redeposition probability is only 6.8×10^{-7}; the redeposition rate only decreases from 1.7×10^{-5} nm/min at 1000 sccm to 7.7×10^{-6} nm/min at 3200 sccm. Such a small change cannot be detected by the QCM and is insignificant next to the etch rate of 0.2 nm/min.
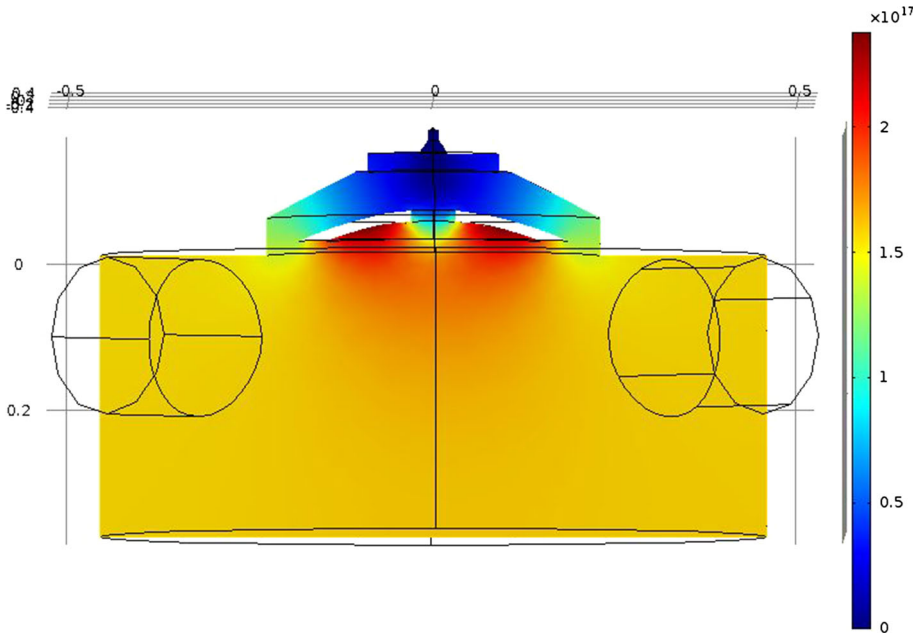
Fig. 12 The simulated SnH_4 density profile from the model in "SnH_4 Transport and Redeposition Theory" section is shown at 325 mTorr, 1000 sccm. At this pressure, the etch rate is 0.2 nm/min, and the temperature is 120 °C. The redeposition coefficient is 6.8×10^{-7}. The peak simulated SnH_4 density at the collector surface is 2.4×10^{17} m^{-3}

Absence of Redeposition in Experiments

Since the only coated-collector etch rates were measured with profilometry on a very thin deposition of Sn in previous works, it was desirable to demonstrate the lack of redeposition by comparing etching of a coated and uncoated collector using a single QCM. Such a comparison showed no measurable difference between etch rates on a Sn-coated collector and on a clean collector. To coat the entire collector, Sn was deposited in the large GALAXY magnetron chamber described in "Experimental Setup" section, with the QCM being coated while positioned on the collector in GALAXY.

Despite precautions taken to minimize oxidation, some bulk oxidation was observed due to poor base pressure in GALAXY, and etch rates for the GALAXY deposition, shown in Figs. 15 and 16, were slower than for the pure XS depositions in "Reactive Ion Etching of Sn" section. As discussed in "Sn Thin Film Deposition" section, oxidized samples deposited in XS yielded lower etch rates; thus, it is thought that oxidation in GALAXY was also responsible for the reduction in etch rate compared to "Reactive Ion Etching of Sn" section.

However, as shown in Fig. 15, etch rates observed on the QCM did not change between a coated and uncoated collector surface, indicating that redeposition was not hampering Sn removal.

Additionally, to further demonstrate that redeposition was not occurring, a flow experiment was undertaken. The flow was varied between 280 and 560 sccm. As shown in Fig. 16, lowering the flow did not decrease the etch rate at all; in fact, the nominal value at
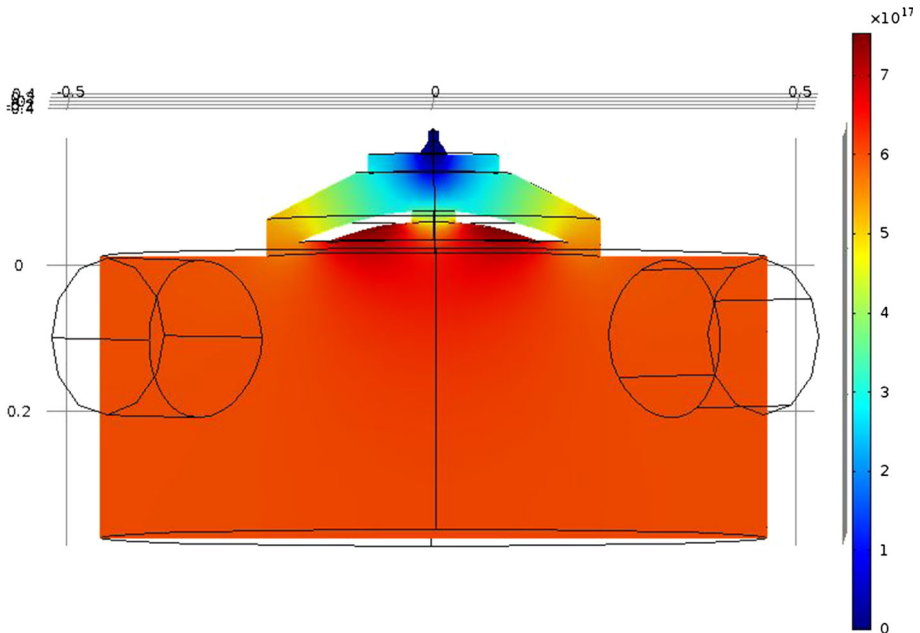
Fig. 13 The simulated SnH_4 density profile is shown at 65 mTorr, 560 sccm. The peak simulated SnH_4 density at the collector surface is 7.7×10^{17} m^{-3}. However, the redeposition rate is increased only to 3.6×10^{-4} nm/min, which is still negligible and does not affect the net removal rate of 1.9 nm/min

a lower flow is slightly higher (though well within error). By showing that higher flow does not raise the removal rate, the lack of redeposition is further confirmed.

As one last check, the QCM was mounted next to the collector rather than on it. Knowing that etching is driven by ion energy flux, a QCM placed next to the collector should see little or no etching; however, it should still experience any deposition that is occurring. Performing this check yielded apparent rates well below the noise floor that showed no dependence on pressure and varied between a nominal deposition rate of 0.03 nm/min and a nominal etch rate of 0.02 nm/min. These results are simply noise and indicate a lack of measurable redeposition. Based on the data in this section, a lack of measurable redeposition predicted by the model is confirmed by experiments. It should be noted that, while SnH_4 is known to not decompose upon impact with itself or H_2, it likely decomposes upon impact with certain plasma species, such as electrons, ions, and H radicals. This is suggested by the presence of a very thin Sn film which appears on areas near the collector that were not bombarded by energetic ions; it is visible only after hours of etching. However, due to the diluted nature of both SnH_4 and the plasma-produced species, the mean free path between these species is quite large and rendered this effect negligible compared to the etch rate.
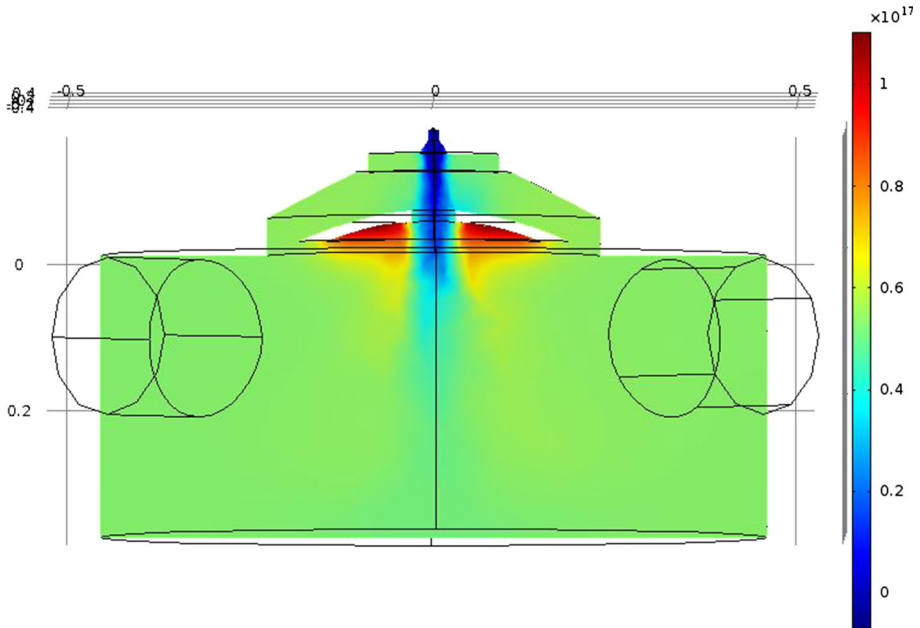
Fig. 14 The simulated SnH_4 density profile is shown at 325 mTorr, 3200 sccm. The peak simulated SnH_4 density at the collector surface is 1.1×10^{17} m^{-3}. However, due to a redeposition probability of 6.8×10^{-7}, the redeposition rate is decreased from 1.7×10^{-5} to 7.7×10^{-6} nm/min. Such a small decrease is insignificant next to the etch rate of 0.2 nm/min and shows that simply increasing flow cannot significantly increase the removal rate; instead, the Sn removal rate is limited by the IEF

Fig. 15 While the impure QCM deposition causes lower etch rates than in previous etches, the same etch rates are seen for both a clean collector and a coated collector. This confirms the predictions of the model, showing that redeposition does not measurable affect etch rates within the parameter space considered
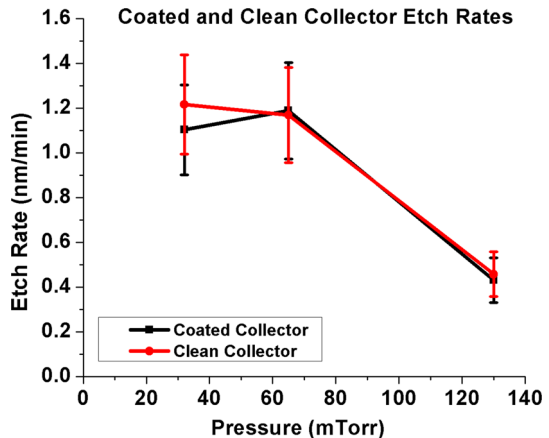
Conclusions

In this paper, an investigation of the mechanism behind Sn etching by an H_2 plasma was then undertaken to determine the limiting factor. It was shown that etch rates in the plasma system did not track radical density. It was shown that etching was strongly dependent on ion energy flux, suggesting a reactive ion etching process where energetic ions break

Fig. 16 Although lowering the flow was confirmed by the model to raise the SnH$_4$ density in the chamber, doing so does not cause redeposition to lower the etch rate. This further confirms a lack of redeposition for the etching conditions in this work
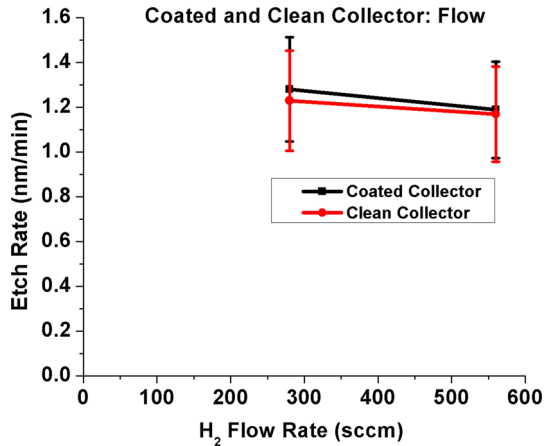
surface bonds and allow radicals to react with the surface material. Etch rate and ion energy flux were both shown to vary linearly with power. Flow did not affect the etch rate of a single QCM nor of etching the entire collector.

The elucidation of ion-enhanced Sn etching presented herein can be extraordinarily useful in the design of EUV collector cleaning systems. The use of energetic ions to activate a Sn surface without sputtering multilayer mirrors can greatly increase the efficiency of hydrogen-based cleaning. One Sn atom is etched for every 2300 incident radicals when low energy ions are present. This etching efficiency is more than an order of magnitude higher than previous estimates of the etching efficiency of radical-only systems (approximately 1 Sn atom per 10^5 incident radicals) [9, 10, 12]. An understanding of the role of energetic ions, combined with the in situ nature of the demonstrated cleaning system and the knowledge that energetic ions can be employed without damaging multilayer mirrors, could allow for great improvements in collector cleaning and collector lifetime.

Additionally, it was shown by a theoretical model and multiple experiments that, within the parameter space explored decomposition of SnH$_4$ and subsequent redeposition of Sn does not play a role in significantly limiting the net removal rate. While SnH$_4$ decomposition does occur, it proceeds with very low probabilities at the temperatures used in EUV collector systems. High rates of flow are not needed to exhaust the SnH$_4$ in EUV systems with cooled collectors.

References

1. Moore GE (1998) Cramming more components onto integrated circuits. Proc IEEE 86(1):82–85
2. Shilov A (2017) Samsung and TSMC roadmaps: 8 and 6 nm added, looking at 22ULP and 12FFC, *Anandtech.com*. http://www.anandtech.com/show/11337/samsung-and-tsmc-roadmaps-12-nm-8-nm-and-6-nm-added. Accessed 24 May 2017

3. Benschop J (2009) EUV: past, present and prospects Jos Benschop. Int Symp Extreme Ultrav Lithogr
4. Burdt RA et al (2010) Laser wavelength effects on the charge state resolved ion energy distributions from laser-produced Sn plasma. J Appl Phys 107(4):043303
5. Kagawa T, Tanuma H, Ohashi H, Nishihara K (2007) RCI simulation for EUV spectra from Sn ions. J Phys: Conf Ser 58:149–152
6. Hecquet C et al (2007) Design, conception and metrology of EUV mirrors for aggressive environments. Damage VUV EUV X-ray Opt 6586:65860X–65860X–10
7. Allain JP et al (2007) Energetic and thermal Sn interactions and their effect on EUVL source collector mirror lifetime at high temperatures. Proc SPIE 6517:65171V–65171V–10
8. Burdt RA (2011) Ion emission and expansion in laser-produced tin plasma, University of California, San Diego (Ph.D. Diss.)
9. van Herpen MMJW, Klunder DJW, Soer WA, Moors R, Banine V (2010) Sn etching with hydrogen radicals to clean EUV optics. Chem Phys Lett 484(4–6):197–199
10. Ugur D, Storm AJ, Verberk R, Brouwer JC, Sloof WG (2012) Generation and decomposition of volatile tin hydrides monitored by in situ quartz crystal microbalances. Chem Phys Lett 552:122–125
11. Ugur D, Storm AJ, Verberk R, Brouwer JC, Sloof WG (2014) Decomposition of SnH_4 molecules on metal and metal-oxide surfaces. Appl Surf Sci 288:673–676
12. Braginsky OV et al (2012) Removal of amorphous C and Sn on Mo: Si multilayer mirror surface in Hydrogen plasma and afterglow. J Appl Phys 111(9):1–5
13. Elg DT, Sporre JR, Panici GA, Srivastava SN, Ruzic DN (2016) In situ collector cleaning and extreme ultraviolet reflectivity restoration by hydrogen plasma for extreme ultraviolet sources. J Vac Sci Technol A Vac Surf Film 34(2):21305
14. Elg DT, Panici GA, Peck JA, Srivastava SN, Ruzic DN (2017) Modeling and measurement of hydrogen radical densities of in situ plasma-based Sn cleaning source. J Micro/Nanolithogr MEMS MOEMS 16(2):23501
15. Mozetič M, Drobnič M, Pregelj A, Zupan K (1996) Determination of density of hydrogen atoms in the ground state. Vacuum 47(6):943–945
16. Mozetic M, Vessel A, Cvelbar U, Ricard A (2006) An iron catalytic probe for determination of the O-atom density in an Ar/O_2 afterglow. Plasma Chem Plasma Process 26(2):103–117
17. Mozetic M, Vesel A, Drenik A, Poberaj I, Babic D (2007) Catalytic probes for measuring H distribution in remote parts of hydrogen plasma reactors. J Nucl Mater 363–365(1–3):1457–1460
18. Ruzic DN (1994) Electric probes for low temperature plasmas. American Vacuum Society Press, New York
19. Tamaru K (1956) The thermal decomposition of tin hydride. J Phys Chem 60(5):610–612
20. Finholt AE, Bond AC, Wilzbach KE, Schlesinger HI (1947) The preparation and some properties of hydrides of elements of the fourth group of the periodic system and of their organic derivatives. J Am Chem Soc 69(11):2692–2696
21. Paneth F, Haken W, Rabinowitech E (1924) Uber die Reindarstellung und EIgenschaften des Zinnwasserstoffs. Berichte der Dtsch Chem Gesellschaft 57:1891–1903
22. Norman AD, Webster JR, Jolly WL (1968) 36. Silane, stannane, silane44, germane449 and stannane-d4. Inorg Synth XI:170–181
23. Elg DT (2016) Removal of tin from extreme ultraviolet collector optics by an in situ hydrogen plasma. University of Illinois at Urbana-Champaign
24. Cho S, Yu J, Kang SK, Shih D-Y (2005) Oxidation study of pure tin and its alloys via electrochemical reduction analysis. J Electron Mater 34(5):635–642
25. Sporre J et al (2012) In-situ Sn contamination removal by hydrogen plasma. Proc SPIE 8322:83222L
26. Sporre JR, Elg D, Ruzic DN, Srivastava SN, Fomenkov IV, Brandt DC (2013) Collector optic in situ Sn removal using hydrogen plasma. Proc SPIE 8679:86792H
27. Faradzhev N, Sidorkin V (2009) Hydrogen mediated transport of Sn to Ru film surface. J Vac Sci Technol A Vac Surf Film 27(2):306
28. Piggott MR (1957) The reduction of oxide films by atomic hydrogen. Acta Crystallogr 10:364–368
29. Meng L, Yu H, Szott MM, McLain JT, Ruzic DN (2014) Downstream plasma transport and metal ionization in a high-powered pulsed-plasma magnetron. J Appl Phys 115(22):223301
30. Zhang P, Hu L, Meegoda JN, Gao S (2015) Micro/nano-pore network analysis of gas flow in shale matrix. Sci Rep 5(1):13501
31. Park SK, Economou DJ (1989) A mathematical model for a plasma-assisted downstream etching reactor. J Appl Phys 66(7):3256–3267
32. Park SSKS, Economou DJ (1990) Numerical simulation of a single-wafer isothermal plasma etching reactor. J Electrochem Soc 137(8):2624–2634

33. Lieberman MA, Lichtenberg AJ (2005) Principles of plasma discharges and materials processing, 2nd edn. Wiley, Hoboken
34. Raizer YP, Shneider MN, Yatsenko NA (1995) Radio-frequency capacitive disscharges. CRC Press, Boca Raton
35. Crijns VMC (2014) Hydrogen atom based tin cleaning. Eindhoven University of Technology, Eindhoven